Effect of iron-group ions on the UV absorption of TiO_2

Kernazhitsky L.[1], Shymanovska V.[1], Naumov V.[1], Chernyak V.[2], Khalyavka T.[3] and Kshnyakin V.[4]

[1]Institute of Physics of NAS, 46 Nauki Ave., 03650 Kyiv, Ukraine, e-mail: kern@iop.kiev.ua
[2]Kiev National University, 2/5 Acad. Glushkov Ave., 03122 Kyiv, Ukraine
[3]Institute for Sorption and Endoecology Problems of NAS, 31 Naumov Ave., 03142 Kyiv, Ukraine
[4]Sumy State Pedagogical University, 87 Romenska St., 40007 Sumy, Ukraine

Received: 06.05.2008

Abstract

The UV absorption spectra of polydisperse rutile (TiO_2) doped by transition metal cations Cr^{3+}, Cu^{2+}, Co^{2+} and Fe^{2+} are investigated at room temperature. It is shown that the fundamental absorption edge of TiO_2 is determined by the two mechanisms of electron transitions: one of them represents a direct forbidden transition and the other an indirect allowed one. The fundamental band gap for the pure rutile is determined to be ΔE = 3.013 eV. The absorption of Fe-doped TiO_2 reveals spectral redistribution near the fundamental edge, while the absorption of Co-doped TiO_2 is strictly similar to that of the pure rutile. Photocatalytic decomposition of organic safranine by means of TiO_2 is also studied. It is found that the pure TiO_2 has higher photocatalytic activity in comparison with the doped compounds. We suppose that the impregnation cations act as traps at the initial stage of reaction but their function changes to that of recombination centres as the photocatalytic process develops.

Key words: titanium dioxide (rutile), transition metal cations, UV absorption spectroscopy, fundamental band gap, photocatalytic activity

PACS: 61.72.Uj, 71.55.Eq, 78.40.Fy, 82.30.Lp
UDC: 535.341

1. Introduction

Titanium dioxide (TiO_2) is a wide-gap n-type semiconductor possessing many unique properties such as high dielectric strength, high reflectivity and photocatalytic reactivity. These attract much interest of researchers and have been extensively explored in connection with practical applications in various technologies: photocatalysis, photovoltaics, sensors, nonlinear optics, electro-chrome devices and many others [1–3].

Due to its polymorphism, TiO_2 can exist in different crystalline modifications: anatase, rutile and brookite, each of which manifesting different electric, magnetic, optical and photocatalytic properties. To a considerable degree, these properties depend

upon the structure of TiO_2, its stoichiometry, preparation methods, size of particles and crystallites, degree of chemical purity, etc.

Two modifications of TiO_2, anatase and rutile, have become most thoroughly investigated with the purpose of preparing high-efficiency photocatalysts. However, applications of pure TiO_2 have inherent limitations since its band gap located in the near-UV range at 3 eV (λ = 410 nm) renders it inactive under the effect of visible light. In order to improve the photoactivity and the response to the visible-range light, doping of TiO_2 with the transition metals such as Cr, Mn, Fe, Co, Cu, Ni and others has been widely employed [3].

The photocatalytic activity of metal-doped TiO_2 depends on many factors, including the dopant concentration, the location of energy levels of dopants in the lattice, their *d*-electronic configuration and distribution of dopants. In addition, electronic and optical properties of the modified TiO_2 are determined by both the methods of preparation of the pure rutile and the methods adopted for its doping with the transition metals [4–6]. In spite of extensive researches on the electronic and optical properties of TiO_2, their link with photocatalytic activity of the modified TiO_2 and a role of different transition metals in the appropriate processes have remained to be clarified.

In our previous work [7] we have studied experimentally the influence of transition metal impurities (Cr, Cu, Co and Fe) on the optical transmission and the absorption spectra of polydisperse rutile in a wide spectral range (from 250 to 700 nm). It has been shown that the optical properties of TiO_2 depend essentially on the nature and amount of doping impurities. In the present work we concentrate on the UV absorption spectra for both the pure rutile and that modified by the iron-group cations (Cr, Cu, Co and Fe), with the emphasis upon the vicinity of fundamental absorption edge in TiO_2. We compare these data with the results obtained for photocatalytic activity of TiO_2 during photocatalytic decomposition of an organic dye, safranine, under UV irradiation.

2. Experimental

2.1. Preparation of samples and their characteristics

For our investigations we synthesized polydisperse samples of pure TiO_2 with nanocrystalline rutile structure, in which the contents of the impurities (Cr, Cu, Co, Fe, Mn and Ni) did not exceed 1×10^{-5} wt. %. The samples were obtained by thermal hydrolysis of hydrochloric acid $TiCl_4$ solutions. Then they were dried and calcined at 300^0C [8]. TiO_2 surface was further modified by the transition metal cations (Cr^{3+}, Cu^{2+}, Co^{2+} and Fe^{2+}) by means of adsorption of the corresponding sulfates from the diluted solutions. Again, these samples were dried and calcined at 300^0C. The sample parameters (the average nanocrystallite size D_{110}, the volume V of the molecular unit of TiO_2 and the axial ratio a/c, with a and c being the cell edges) were additionally determined with X-ray diffraction method. The cation-dopant contents were measured using X-ray fluorescence technique (see Table 1).

Table 1. Characteristics of TiO_2 samples under investigation.

Sample	Dopant contents, at. %	$D_{110,}$ Å	$V = ac^2/2$, Å^3	c/a
R	–	207.6	31.28	0.64
R/Fe	6.30	146.6	31.05	0.65
R/Cr	2.77	356.9	31.29	0.64
R/Co	7.04	288.2	31.04	0.65
R/Cu	12.45	97.7	31.36	0.67

The samples for the UV spectroscopic measurements were tableted using KBr (the contents of TiO_2 being 0.1 wt. %). The specific surface of catalyst for the samples was determined using low-temperature argon desorption method.

2.2. Optical measurements

In order to study the optical properties of TiO_2, we applied a classic method of UV absorption spectroscopy [7]. The spectra were measured with a portable and rapid PC-operated CCD-based multi-channel optical spectrum analyzer SOLAR SL40 (the grating 600 l/mm, the blaze 350 nm, the 3648-pixel TCD1304AP linear sensor, the time response 7 ms and the accumulation time up to 10 s). It had a wide working range (200–1100 nm) and a spectral resolution of ~ 0.5 nm. For spectral calibration, a set of etalon spectral lamps was used, including mercury, deuterium, xenon and tungsten lamps. The deuterium lamp DDC-30 (λ_{1max} = 245 nm and λ_{2max} = 311 nm) served as a probing UV light source. The optical images (signals) were normally focused by quartz lens, through a fine optical fibre with microlens, from the samples directly onto the entrance slit of our spectral device. All the spectra (both transmission and absorption ones) were measured in the same experimental geometry and under the same conditions (room temperature). They were compared using a standard statistical treatment.

2.3. Photocatalytic measurements

We chose safranine dye ($C_{20}H_{19}ClN_4$) as a model organic liquid for evaluating the photocatalytic activity of TiO_2 samples prepared by us. Investigations of photocatalytic degradation of the safranine were performed in a quartz tube reactor at room temperature. A standard mercury lamp BUV-30 was used when UV-irradiating the dye solution. The reactor was settled at the distance of 1 cm from the lamp. The solution was mixed with a magnetic stirrer during the irradiation (the speed of rotation being 120 rpm). The initial dye concentration was 0.3 g/l and the concentration of TiO_2 was 6 g/l. The solution volume in the reactor tube was equal to 50 ml. The probes of the reaction mixture were taken at definite time moments for checking the process. The solid phase was separated from the liquid with a centrifuge (8000 rpm). The changes in the safranine concentration

during the photocatalysis were determined with the aid of standard LOMO spectrophotometer.

3. Results and discussion

3.1. Absorption spectra of the pure and modified TiO_2

The absorption spectra of the pure rutile samples (R300) and the rutile doped with the transition metals (R300/Cr, R300/Cu, R300/Co and R300/Fe) were measured in the wavelength range of λ = 220–500 nm. Fig. 1 and 2 show the absorption coefficients near the fundamental edge (~3 eV) respectively in the regions of low (2.75–3.0 eV) and high (3.0–3.8 eV) photon energies. The absorption edge of TiO_2 is clearly observed.

Let us emphasize the following features of the absorption curves (see Fig. 1). The absorption tail is observed in the region of $h\omega$ = 2.8–3.0 eV, whereas a strong absorption appears at the energies $h\omega > 3$ eV. The absorption curves behave in a nonmonotonic manner with increasing $h\omega$, the corresponding changes being especially notable in the region of 2.95–3.10 eV. The most noticeable step-like changes in the absorption curves are marked by arrows in Fig. 1.

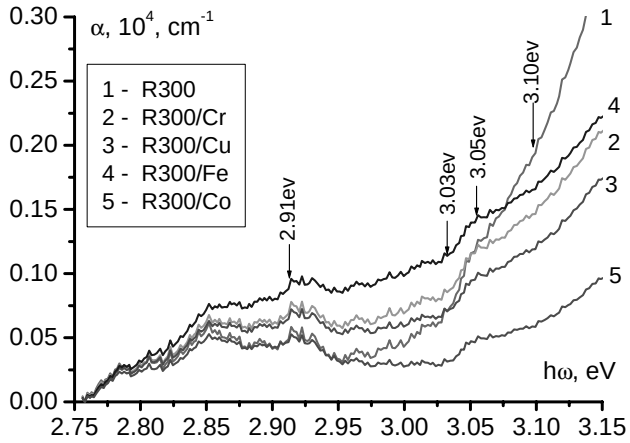

Fig. 1. Absorption spectra of the pure and doped rutile at room temperature near the fundamental edge at lower photon energies

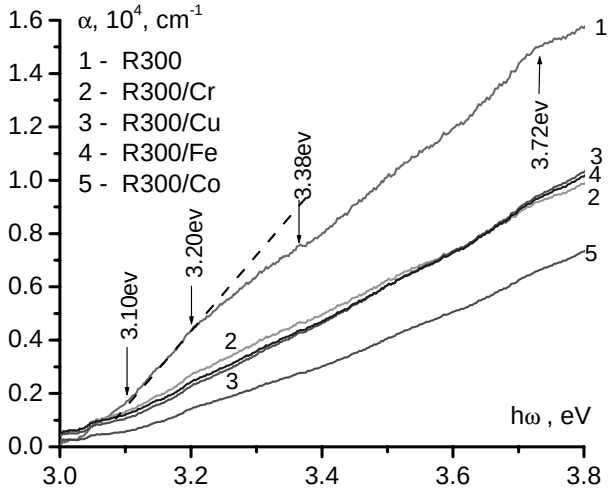

Fig. 2. Absorption spectra of the pure and doped rutile at room temperature near the fundamental edge at higher photon energies.

The same changes in the absorption coefficient have been observed in the experiments [9, 10] with single rutile crystals performed at the temperatures 1.6–200 K. These features have been identified as a manifestation of direct and indirect transitions from the valance band to the conduction one. Therefore we assume that the mechanisms of photon absorption in the polycrystalline rutile are similar to those peculiar for the single crystal. According to the sketch of energy levels given in [11], the features mentioned above can be related to the intrinsic absorption edge for TiO_2 crystals and the direct and indirect energy gaps E_g, as shown in Fig. 3.

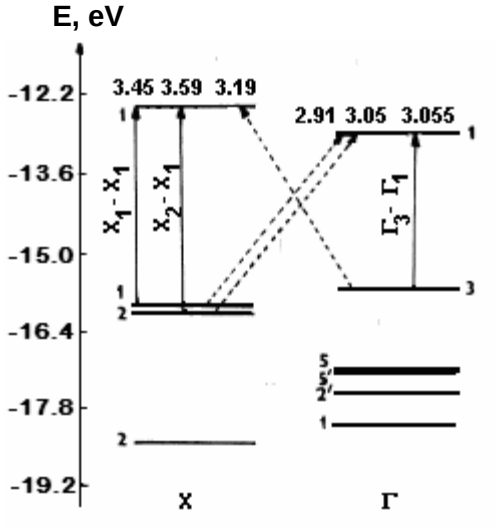

Fig. 3. Sketch of direct and indirect transitions in the rutile according to [11].

So, the transition marked by arrow at 2.91 eV in Fig. 1 can be assigned to the indirect allowed transition X_1–Γ_1, while that occurring at 3.03–3.055 eV can be assigned to a direct forbidden transition (namely, Γ_3–Γ_1) [9]. At the room temperature, this direct gap is evaluated as 3.062 eV. The transition located between 3.055 and 3.10 eV should be compared with the data for the indirect gap at low temperatures: 3.049 eV and 3.051 eV [9, 10]. According to [9], this is the allowed transition X_2–Γ_1, though smeared with increasing temperature and shifted to the 'red' side.

Fig. 2 shows the absorption coefficient for TiO_2 at the higher photon energies ($h\omega$ =3.1–3.8 eV). Here some slope changes in the absorption curves are also labelled by arrows. The transition at 3.10–3.20 eV could be explained as the indirect allowed transition Γ_3–X_1 (Fig. 3), which has also been observed at 3.11–3.13 eV in the work [12]. We assume that the higher-energy transitions in the regions of 3.20–3.38 eV and 3.38–3.72 eV should be interpreted as direct allowed ones. According to the results [11], these transitions are X_1–X_1 (3.45 eV with $E \perp c$) and X_2–X_1 (3.59 eV with $E \| c$).

The spectral dependences of the absorption of TiO_2 shows that the doping with different transition metals affects in different ways the magnitude of absorption coefficient around the fundamental edge at 3 eV. For the spectral region defined by $h\omega < 3$ eV, doping with Co cations does not influence the absorption at all, whereas doping with Cu, Cr and Fe cations increases the absorption of TiO_2 very much. So, at

$h\omega$ = 2.95 eV the absorption of the rutile doped by Cu (or Cr) and Fe is respectively two and four times larger, when compare with that of the undoped rutile. In the energy region $h\omega > 3$ eV, the doping decreases the absorption in comparison with the undoped rutile.

Thus, one can state that the doping concerned with R300/Co samples result in no absorption redistribution inside the visible range, while the dopings with Cr, Cu and Fe substantially increase the absorption of TiO_2 in the long-wavelength region. When re-calculating the identical dopant concentrations in the spectral region under test ($h\omega$ = 2.8–3.0 eV or λ = 443–413 nm), we assume that the Cr and Fe dopants are twice as much efficient when compare with the Cu dopant.

Our experiments have shown that the absorption spectra of Cr- and Cu-doped TiO_2 in this region are similar. According to [13], the t_{2g} level of Cr is located in the middle of the band gap. Therefore we assume that the level t_{2g} of Cu impurity is to be located in the middle of the band gap, too. The absorption spectrum of Co-doped TiO_2 near the fundamental edge (2.8–3.0 eV) is strictly similar to that of the pure TiO_2. This result coincides with the data [14]. Finally, Fe-doped TiO_2 shows noticeable absorption redistribution in the long-wavelength region due to the transitions from the t_{2g} level, which can be populated from the impurity band tail [13].

3.2. Fundamental band gap

The fundamental band gap represents a principal characteristic of TiO_2 semiconductor. In our case it is attributed to the inter-band transitions of electrons between the highest occupied 2*p* states of O in the valence band and the lowest unoccupied 3*d* states of Ti with the character t_{2g} in the conduction band. As mentioned above, the extended absorption-edge spectrum for the rutile suggests a possibility of both direct and indirect transitions. According to [15], the dependence of the absorption coefficient for the forbidden direct transitions Γ_3–Γ_1 in the region of $h\omega$ = 3.03–3.055 eV can be described by the equation

$$\alpha \sim (h\omega - E_{gd})^r, \tag{1}$$

where $h\omega$ is the photon energy, $E_{gd} = \Delta E_0$ the direct band gap and the index r is equal to $r = 3/2$. Then the plots of $\alpha^{2/3}$ versus $h\omega$ would be straight lines, as shown in Fig. 4 in the area of dotted lines.

We have estimated the fundamental band gap energies ($\Delta E_0 = E_{gd}$) from the intercept of tangents of the plots. The best-fit values E_{gd} are presented in Table 2. The band gap energies corresponding to the indirect allowed transitions X_2–Γ_1 in the region of $h\omega$ = 3.055–3.10 eV might be estimated in a similar manner, using the plots of $\alpha^{1/2}$ versus $h\omega$ (see Fig. 5).

In this case we deal with the transitions forming free excitons [16], so that we have

$$\Delta E = E_{gi} \pm h\Omega, \tag{2}$$

where the signs "+" and "–" denote respectively the absorption and emission of phonons, E_{gi} is the indirect band gap, $h\Omega$ the phonon energy and the index r in Eq. (1) is equal to

$r = 2$. The direct and indirect band edge values (ΔE_{exp}) have been evaluated from the experimental plots of α vs $h\omega$, as shown in Fig. 1 and 2 (see also the data represented in Table 2).

Recently *Bak et al.* [17] have derived the ΔE data for the single crystals and ceramics of TiO_2, using both the optical and electric methods and additional theoretical calculations. The scatter of ΔE data yields the average value equal to $\Delta E = 3.039 \pm 0.053$ eV. This agrees well with our value $\Delta E = 3.013$ eV (see Table 2) obtained for the polydisperse crystalline rutile at the room temperature.

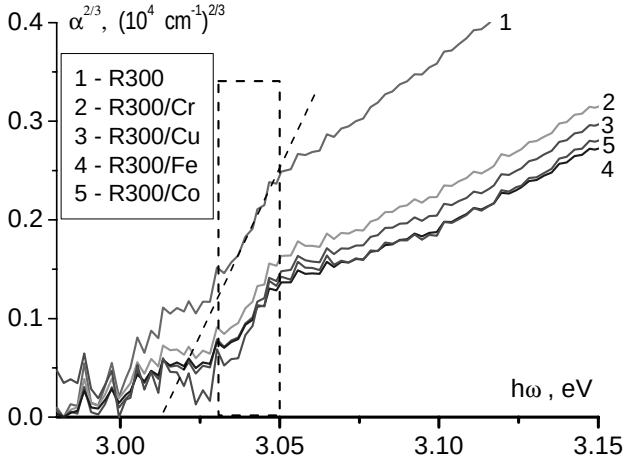

Fig. 4. Absorption spectra of the pure and doped rutile at room temperature, plotted as $\alpha^{2/3}$ vs the photon energy.

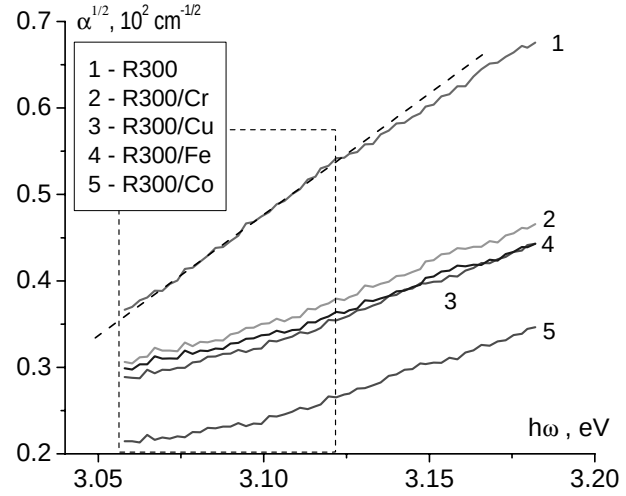

Fig. 5. Absorption spectra of the pure and doped rutile at the room temperature, plotted as $\alpha^{1/2}$ vs the photon energy.

Our results allow making some assumptions about possible mechanisms of exciton-phonon interaction in the pure and doped TiO_2. Let us consider the ΔE parameter for the case of indirect transitions. Taking into account the ΔE_{exp} and E_{gi} values for the pure rutile (Table 2), one can obtain $h\Omega = 108$ meV on the basis of Eq. (2). This conforms satisfactorily to the phonon parameter $h\Omega = 102$ meV, thus assisting the indirect transition in TiO_2 [18]. However, similar estimations for the modified TiO_2 testify that the

Table 2. Experimental and calculated band gap parameters for the pure and modified TiO_2.

Sample	Direct band gap		Indirect band gap	
	ΔE_{exp}, eV	E_{gd}, eV	ΔE_{exp}, eV	E_{gi}, eV
R300	3.02	3.013	3.048	2.94
R300/Fe	3.00	3.018	3.047	2.69
R300/Cr	2.98	3.018	3.046	2.78
R300/Co	3.04	3.028	3.047	2.67
R300/Cu	3.02	3.024	3.047	2.76

phonon energies in this case must be very large (250–300 meV). In fact, no strong phonon structure with this energy exists. It should certainly correspond to some other mechanism of exciton-phonon coupling. We suppose that the doping of rutile by the transition metals would result in worsening crystal structure of TiO_2. This can increase the exciton-phonon coupling constant (g), thus leading to capture of excitons by phonons. The critical exciton-phonon coupling constant for the indirect edge of rutile is $g_c = 0.95$ [21]. The self-trapping of excitons occurs when $g > g_c$ [22]. Our estimates show that this condition for the self-trapping of excitons can be fulfilled for the modified rutile, while for the pure rutile one has $g = 0.94$ [10] and so the excitons are mostly free.

3.3. Photocatalytic activity of the pure and modified rutile

We have studied the reaction of safranine degradation as a model for evaluating the photocatalytic activity of the pure and modified TiO_2. Our results for the photocatalytic degradation of safranine under the UV irradiation are depicted in Fig. 6 and summarized in Table 3. Without any catalyst, the rate has remained low, with the permanent rate constant $k_d = 0.29\times10^{-4}$ s^{-1}.

Adding of TiO_2 catalyst yields in increasing safranine degradation rate in the first 30 min for all the samples, except for the Fe-doped TiO_2. The pure TiO_2 exhibits the best photocatalytic activity, with the rate constant $k_{d1} = 3.24\times10^{-4}$ s^{-1} being more than 10 times higher than that observed without any catalyst. In general, the degradation rate constant k_{d1} decreases in the following row: R300 > R300/Co > R300/Cu >> R300/Fe, i.e. the safranine degradation rate becomes the least for the case of Fe-doped TiO_2.

Table 3. Degradation rate constants for safranine with TiO_2 catalysts.

Catalyst	$k_{d1}\times10^4$, s^{-1}	$k_{d2}\times10^4$, s^{-1}
–	0.29	0.29
R300	3.24	0.34
R300/Fe	0.26	0.63
R300/Co	2.68	0.26
R300/Cu	2.07	0.24

During the next 30–180 min, the photocatalytic activity decreases and the degradation rates for all of the samples become comparable with the rate occurred in the absence of catalyst, while the k_{d2} parameter for the Fe-doped TiO_2 increases more than twice.

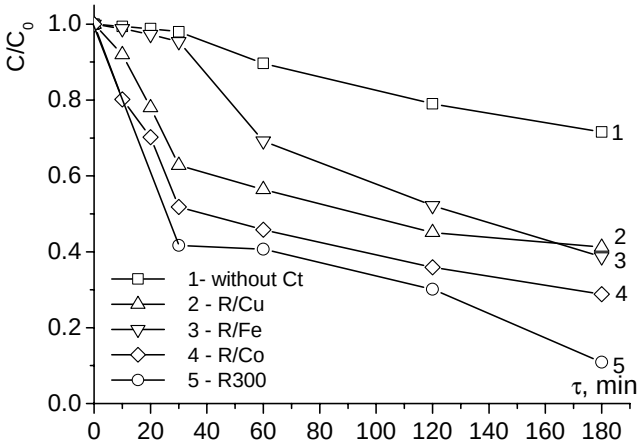

Fig. 6. Photocatalytic degradation of safranine.

The photocatalytic activity of TiO_2 depends on competition between the rate of transferring surface charge carriers from the bulk to the surface and the recombination rate of photo-generated electrons and holes. The recombination process decreases the lifetime of separated electron-hole pairs during the photocatalytic reaction. If compare to some other semiconductors, the surface charge carriers in TiO_2 are relatively long-lived (~ 250 ns), thus allowing the electrons or holes to achieve the surface of particles [23]. In the photocatalysis with TiO_2, oxygen plays a significant part. It has been suggested that O_2 molecules adsorbed are efficient electron traps in the conduction band, which hinder electron-hole recombination [24, 25].

The difference in the behaviours of Fe-doped TiO_2, on the one side, and of Cu- and Co-doped TiO_2, on the other side, could be explained by the fact that the iron ions have special features distinguishing them from the other metallic dopants [3]. The Fe ions in TiO_2 can exist in three valence states; two of them, Fe^{2+} and Fe^{4+}, being relatively unstable, though Fe^{3+} have a half-filled d^5 orbital, which is known to be more stable. When these ions trap photo-generated electrons and holes under the irradiation, the half-filled electronic configuration is destroyed; its stability decreases and the unstable ions Fe^{2+} and Fe^{4+} appear:

$$Fe^{3+} + Ti^{3+} \rightarrow Fe^{2+} + Ti^{4+} \qquad \text{(electron trap)},$$
$$Fe^{3+} + O^{-} \rightarrow Fe^{4+} + O^{2-} \qquad \text{(hole trap)}.$$

The electrons and holes so trapped can easily be transferred to the oxygen and OH-group adsorbed on the catalyst surface. Then the Fe ions return to their original stable half-filled electron structure:

$$Fe^{4+} + OH^{-} \rightarrow Fe^{3+} + OH^{\bullet} \qquad \text{(hole release)},$$
$$Fe^{2+} + O_2 \rightarrow Fe^{3+} + O^{-}_2 \qquad \text{(electron release)}.$$

This might promote charge transfer and efficient separation of electrons and holes. *Zhou et al.* [26] have demonstrated that the photocatalytic activity of Fe-doped TiO_2 is strongly dependent on the dopant concentration (0.05–2.5 at. %), since the Fe^{3+} ions can serve not only as mediators of the interfacial charge transfer but also as recombination centres. In our case the Fe-dopant concentration has been equal to 6.30 at. %, obviously causing high recombination rate for the photo-generated electrons and holes.

Thus, we suppose that the main reason for the rapid increase in the reaction rate at the initial stage is that the impregnated metal cations function as traps of the photo-excited electrons. Consequently, they retard the recombination step at the initial stage of

the reaction cycle. At the next stage of the photocatalytic process, their role is changed to that of the recombination centres.

4. Conclusions

We have studied the UV absorption spectra for the pure and modified polydisperse rutile at the room temperature and have found the following regularities summarized below:

(i) The fundamental absorption edge of the polydisperse rutile is formed by the two mechanisms, the direct forbidden transition and the indirect allowed transition.

(ii) The fundamental band gap energy derived by us for the pure TiO_2 (ΔE = 3.013 eV) is in a good agreement with the reference data.

(iii) The absorption of the Fe-doped TiO_2 reveals the most noticeable spectral redistribution near the fundamental edge within the range of 2.8–3.0 eV, while the absorption spectrum for the Co-doped TiO_2 is similar to that of the pure rutile.

(iv) Modification of the rutile by the transition-metal cations results in increasing exciton-phonon coupling and a capture of excitons by phonons.

(v) In the reaction of photocatalytic degradation of the organic dye (safranine), the pure TiO_2 has higher photocatalytic activity than the metal-doped TiO_2. We suppose that the impregnated cations act as exciton traps at the initial reaction stage but they change their function to recombination centres as the photocatalysis proceeds further on.

Acknowledgement

This work is supported by the Ministry of Education and Science of Ukraine and by the National Academy of Sciences of Ukraine (under the Program VC 138/23).

References

1. Mills A and Hunte S, 1997. An overview of semiconductor photocatalysis. J. Photochem. Photobiol. A Chem. **108:** 1–35.
2. Diebold U, 2003. The surface science of titanium dioxide. Surf. Sci. Rep. **48**: 53–229.
3. Carp O, Huisman C L and Reller A, 2004. Photoinduced reactivity of titanium dioxide. Prog. Solid State Chem. **32**: 33–177.
4. Hermann J M, Disdier J and Pichat P, 1984. Effect of chromium doping on the electrical and catalytic properties of powder titania under UV and visible illumination. Chem. Phys. Lett. **108**: 618–622.
5. Karakitsou K E and Verykios X E, 1993. Effect of altervalent cation doping of TiO_2 on its performance as a photocatalyst for water cleavage. J. Phys. Chem. **97**: 1184–1189.
6. Mu W, Herrmann J M and Pichat P, 1989. Room temperature photocatalyst oxidation of liquid cyclohexane into cyclohexanone over neat and modified TiO_2. Catal. Lett. **3**: 73–84.
7. Kernazhitsky L, Shymanovskaya V, Puchkovska G, Naumov V, Chernyak V, Prysiazhnevych I and Yukhimenko V, 2008. Influence of transition metal impurities on polydisperse rutile absorption spectra. J. Optoel. & Adv. Mater. (at press).
8. Melnyk V, Shymanovska V, Puchkovska G, Bezrodna T and Klishevich G, 2005.

Low-temperature luminescence of different TiO_2 modifications. J. Mol. Struct. **573**: 744–747.
9. Pascual J, Camassel J and Mathieu H, 1978. Fine structure in the intrinsic absorption edge of TiO_2. Phys. Rev. B. **18**: 5606–5614.
10. Tang H, Levy F, Berger H and Schmid P E, 1995. Urbach tail of anatase TiO_2. Phys. Rev. B. **52**: 7771–7774.
11. Daude N, Gout C and Jouanin C, 1977. Electronic band structure of titanium diooxide. Phys. Rev. B. **15**: 3229–3235.
12. Vos K and Krusemeyer H J, 1975. Low temperature electroreflectance of TiO_2. Solid State Commun. **15**: 949–952.
13. Umebayashi T, Yamaki T, Itoh H and Asai K, 2002. Analysis of electronic structures of 3d transition metals-doped TiO_2 based on band calculations. J. Phys. Chem. Sol. **63**: 1909–1920.
14. Wang Y, Cheng H, Hao Y, Ma J, Li W and Cai S, 1999. Preparation, characterization and photoelectric behaviors of Fe(III) doped TiO_2 nanoparticles. J. Mater. Sci. **34**: 3721–3729.
15. Tauc J, Optical Properties of Solids. Amsterdam: North-Holland (1970).
16. Elliot R.J, 1957. Intensity of optical absorption by excitons. Phys. Rev. **108**: 1384–1389.
17. Bak T, Nowotny J, Rekas M and Sorrell C C, 2003. Defect chemistry and semiconducting properties of titanium dioxide: I. Intrinsic electronic equilibrium. J. Phys. Chem. Sol. **64**: 1043–1056.
18. Porto S P S, Fleury P A and Damen T C, 1967. Raman spectra of TiO_2, MgF_2, ZnF_2, FeF_2, and MnF_2. Phys. Rev. **154**: 522–526.
19. Dow J D, 1972. Toward a unified theory of Urbach's rule and exponential absorption edges. Phys. Rev. B **5**: 594–610.
20. Cho K and Toyozawa Y, 1971. Exciton-phonon interaction and optical spectra: self-trapping, zero-phonon line and phonon sidebands. J. Phys. Soc. Jpn. **30**: 1555–1574.
21. Tang H, Berger H, Schmid P E, Levy F and Burri G, 1993. Photoluminescence in TiO_2 anatase single crystals. Solid State Commun. **87**: 847–850.
22. Schrieber M and Toyozawa Y, 1982. Numerical experiments on the absorption lineshape of the exciton under lattice vibrations. I. The Overall Lineshape. J. Phys. Soc. Japan. **51**: 1528–1536.
23. Ovenstone J, 2001. Preparation of novel titania photocatalysts with high activity. J. Mater. Sci. **36**: 1325–1329.
24. Linsebliger A L, Lu G and Yates J T, 1995. Photocatalysis on TiO_2 surfaces: principles, mechanisms, and selected results. Chem. Rev. **95**: 735–758.
25. Hofmann M R, Martin S T, Choi W and Bahnemann D W, 1995. Environmental applications of semiconductor photocatalysis. Chem. Rev. **95**: 69–96.
26. Zhou M, Yu J and Cheng B, 2006. Effect of Fe-doping on photocatalytic activity of mesoporous TiO_2 powders prepared by an ultrasonic method. J. Hazard. Mater. B. **137**: 1838–1847.